

Astron 128 - Lab 0: Stellar Clusters And Their Properties

SHRIHAN AGARWAL ¹

¹ *University of California, Berkeley, Department of Astronomy, Berkeley, CA 94720*

1. INTRODUCTION

In this lab, we construct HR diagrams of the Hyades, M67, and NGC6397 clusters and investigate their properties, including age, metallicity, and more. In order to generate these, we utilize GAIA DR3 magnitudes, parallax and proper motion data extracted from the DR3 database¹. We apply multiple quality cuts on the DR3 dataset using AQDL queries, as described further in Section 2. We then make further cuts on parallax in Section 3, and proper motion in Section 4. Using these cuts, the final result is shown in HR Diagrams in Section 5. We then compared these HR diagrams to synthetic CMDs using MIST (Section 6) and PARSEC (Section 7).

2. GAIA: EXTRACTING DATA WITH AQDL

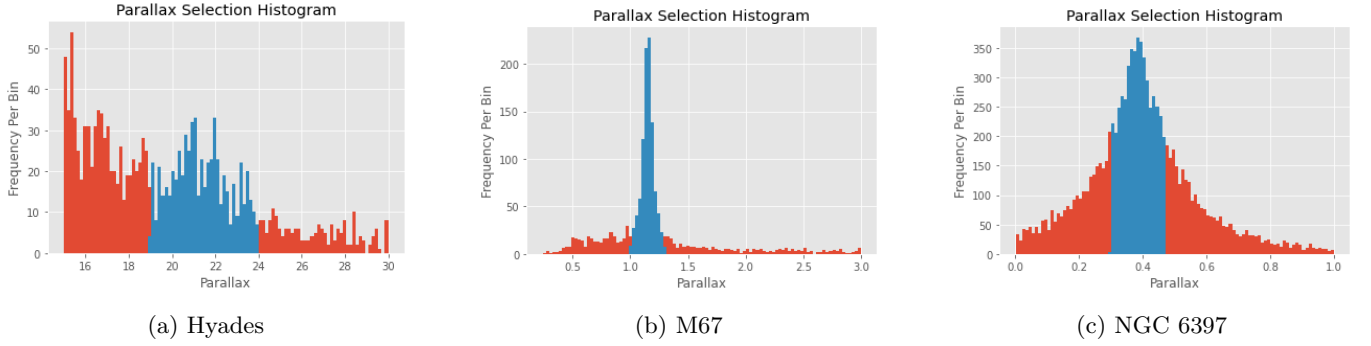
We utilize SIMBAD (Wenger et al. 2000) for identifying centers of stellar clusters, as well as providing proper motion and parallax priors, as seen in Sections 3, 4. This initial cluster center is used to begin a cone search query on the GAIA DR3 database, ordered by angular separation from query center, with a large radius. We follow Gaia Collaboration et al. (2018) for the majority of the quality cuts on stars retrieved from GAIA. This includes the following cuts in Gaia AQDL Queries:

- `phot_g_mean_flux_over_error > 50`
- `phot_rp_mean_flux_over_error > 20`
- `phot_bp_mean_flux_over_error > 20`
- `visibility_periods_used > 8`
- `astrometric_chi2_al/(astrometric_n_good_obs_al-5) < 1.44 * greatest(1,exp(-0.4*(phot_g_mean_mag-19.5)))`
- `phot_bp_rp_excess_factor < 1.3+0.06*power(phot_bp_mean_mag-phot_rp_mean_mag,2)`
- `phot_bp_rp_excess_factor > 1.0+0.015*power(phot_bp_mean_mag-phot_rp_mean_mag,2)`
- `astrometric_excess_noise < 1`

The exact query is provided along with the code in the submissions for reproducibility. In brief, these cuts eliminate stars for which GAIA had few visibility periods, or otherwise uncertain parallax, proper motion, or magnitude estimates. For further information regarding the reasoning for the quality cuts performed, see Gaia Collaboration et al. (2018).

Table 1: Summary of Search Parameters

| Name | RA | Dec | Search Cone Radius ($^{\circ}$) | Initial Parallax Bounds | Parallax Bounds | PM RA Bounds | PM Dec Bounds |
|----------|-------------|-------------|-----------------------------------|-------------------------|-----------------|--------------|---------------|
| Hyades | 4:29:47.3 | +16:56:53 | 15 | [15, 30] | [19, 24] | [65, 125] | [-50, 0] |
| M67 | 08:51:23.0 | +11:48:50 | 0.5 | [0, 3] | [1.0, 1.3] | [-13, -10] | [-3.8, -2] |
| NGC 6397 | 17:40:42.09 | -53:40:27.6 | 0.5 | [0, 1] | [0.32, 0.47] | [2, 4.5] | [-19, -16] |

**Figure 1:** Parallax selections for Hyades, M67, and NGC 6397, after initial parallax bounds. Exact bounds are specified in Table 1.

Much of the initial stellar selection required exploration and iteration for each of the different clusters. In the initial GAIA query, we settled on specific modifications in order to get accurate data for each cluster. This is provided in Table 1. Here, the RA, Dec, Cone Radius, and Initial Parallax Bounds are present in the GAIA query, limiting the stars we see in the exploration of the dataset. Following which, we decide on final bounds on Parallax and Proper Motion (see 3, 4).

3. PARALLAX SELECTION

We select carefully on parallax. With our initial parallax bounds on GAIA, based on SIMBAD data, we generate a histogram and search by eye for any abnormal jumps in density, indicative of a cluster. The final parallax bounds are highlighted for the clusters in question in Figure 1, and shown in Table 1.

For Hyades, no clear peak could be seen, due to the low number of stars in the cluster. For this case, we simply took a reasonable bounds around the cluster parallax suggested in SIMBAD of 21.059, by taking a range of 19-24. This continued to produce consistent results in proper motion space as well. For M67, a clear peak in parallax was visible, and easily selected on, ranging from 1.0-1.3. For NGC 6397, a broad range of parallax could be visible. This might have just been due to the nature of the large cluster. However, to avoid grabbing stars outside the cluster near 0 parallax, we took a conservative region around the peak, 0.32-0.47.

4. PROPER MOTION SELECTION

Following the parallax selection, we can generally see very clear clusters for proper motion selection. We spread the remaining stars in proper motion space, and search for any clusters. Although a clustering algorithm would be a more principled approach, we found it unnecessary in terms of impact to the quality of the result. We believe that a careful visual inspection based selection should be sufficient for our purpose below.

We generate a scatter-plot and density plot, and make a box selection in proper-motion space for each cluster. While this was easy for M67 and NGC 6397 as they could be easily distinguished from other stars through proper motion, the Hyades cluster has only a few hundred stars. As such, the cluster is hard to select on. The density plots are a

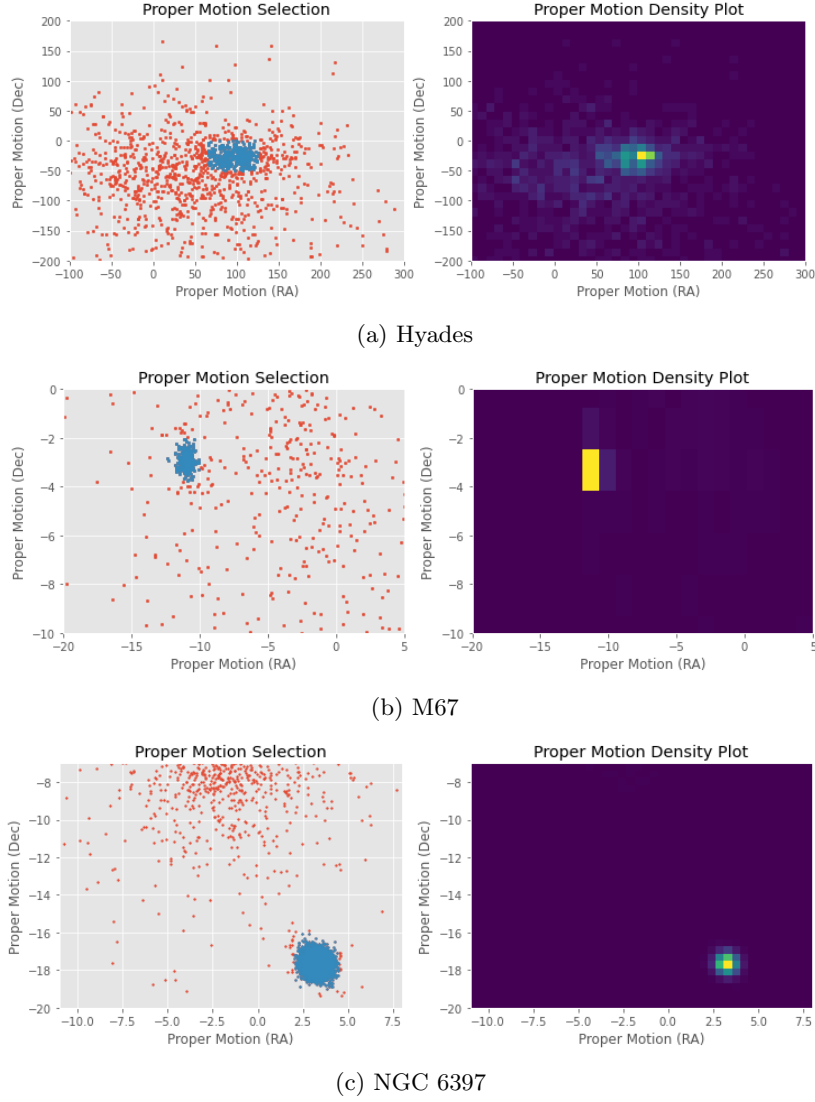


Figure 2: Hyades, M67, and NGC 6397, spread in proper motion space, along with a density distribution. Exact bounds are specified in Table 1.

great aid here, and we take a conservative set of proper motions ($[65, -50] - [125, 0]$). All selections are presented in 1 and plots of density and selected stars are also shown 2.

5. COLOR-MAGNITUDE DIAGRAM GENERATION

Stars which pass both cuts on parallax and proper motion are then presented on a Color-Magnitude Diagram. We present the stars that have passed these more stringent cuts, and compare them on-sky to the stars that have not passed the cuts in Figure 3. Visually, we can compare the clusters to SDSS imaging as a check, and they seem somewhat akin to expectations. We note that the cone search appears elliptical due to the axis scaling, even though we searched a circular area on sky.

The color-magnitude diagrams are presented as in [Gaia Collaboration et al. \(2018\)](#). We utilize the GAIA BP and RP filters in order to calculate the color, and use the GAIA G filter for the apparent magnitude. The apparent magnitude is converted to an absolute magnitude using,

$$M_G = G + 5 + 5 * \log(\omega/1000)$$

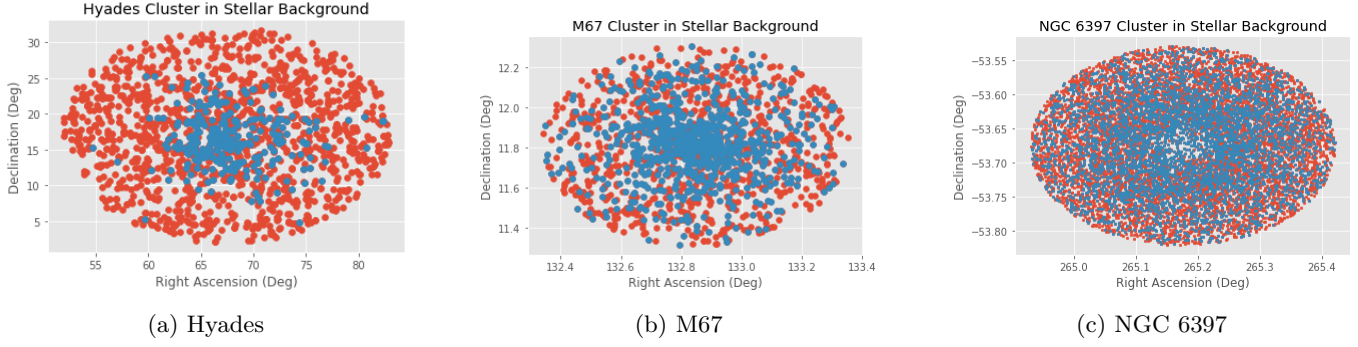


Figure 3: Hyades, M67, and NGC 6397, spread in RA-Dec space, as if viewed on sky. Visually, we can see evidence of a cluster similar to those seen in SDSS.

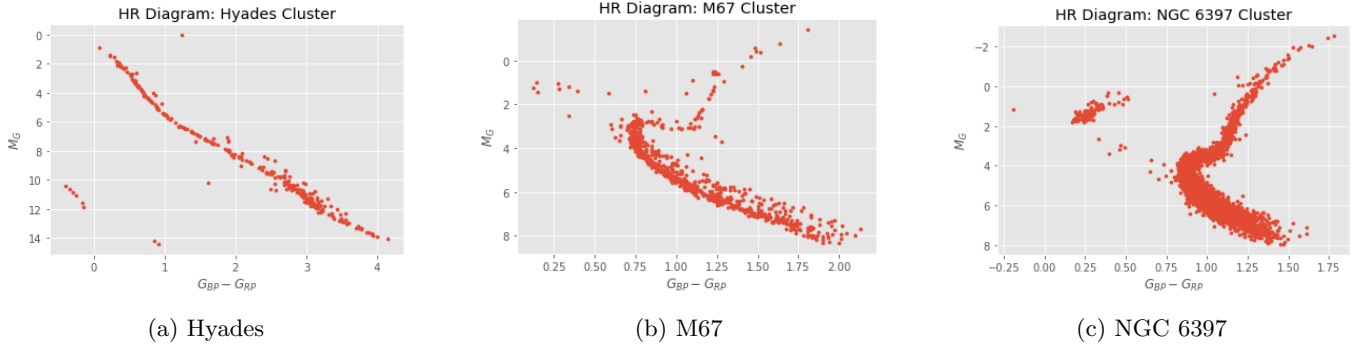


Figure 4: Hyades, M67, and NGC 6397, presented in color magnitude diagrams.

where ω is the estimated parallax of the star in question. In terms of GAIA AQDL query, `phot_g_mean_mag+5*log10(parallax)-10 as mg` was used to get the G band absolute magnitude of the star, M_G . The color-magnitude diagram is presented in Figure 4.

We can see a clear turn-off point from the main-sequence in the older M67 and NGC6397 clusters, but so not see them in the Hyades cluster, as expected. We can understand more with comparisons to synthetic isochrone models such as MIST and PARSEC.

6. MIST ISOCHRONE COMPARISONS

For the MIST Isochrones, we use prior information from earlier papers in the topic. We took a range of metallicities, from the prior ± 0.3 , and a range of ages, from the papers with a $\log \text{Age} \pm 1$. For example, for Hyades, we took a range in $\log \text{Age}$ from 8-9, for M67, from 9-10, and for NGC 6397, from 9.3-10.3, all with steps of 0.1, which hit the upper limit of the isochrones available from MIST.

We checked a variety of ages and metallicities by eye to determine the best fit age and metallicity. Plots of the following are shown for Hyades in Figure 6. The final isochrone chosen for the Hyades cluster was of metallicity 0.2 ± 0.1 , while the $\log(\text{Age})$ was 8.7 ± 0.05 , corresponding to a age of about 500 Myr.

Similar plots are shown for M67 and NGC 6397. For M67, we found a best-fit metallicity of 0.2 ± 0.1 , and a $\log(\text{Age})$ of 9.6 ± 0.05 , corresponding to an age of about 4Gyr. For the metal-poor NGC 6397, we found a best fit metallicity of -2.2, and a $\log(\text{Age})$ of 10.1 ± 0.05 , making it the oldest cluster with an age of 12.6Gyr. Plots for these are shown in Figure 7 and Figure 8.

This was done using GAIA synthetic photometry provided by MIST, with most settings set to default. On extinction, we used results of past papers to choose an A_V of 0.12 for M67 and an A_V of 0.68 for NGC 6397. The extinction for the Hyades cluster was deemed negligible and left at 0.

7. PARSEC ISOCHRONE COMPARISONS

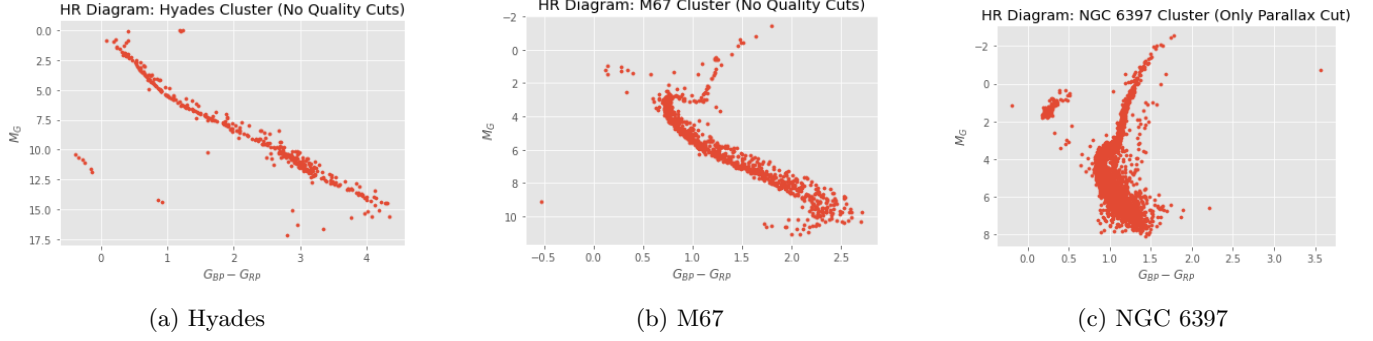


Figure 5: Hyades, M67, and NGC 6397, presented in color magnitude diagrams, before quality cuts were applied based on [Gaia Collaboration et al. \(2018\)](#).

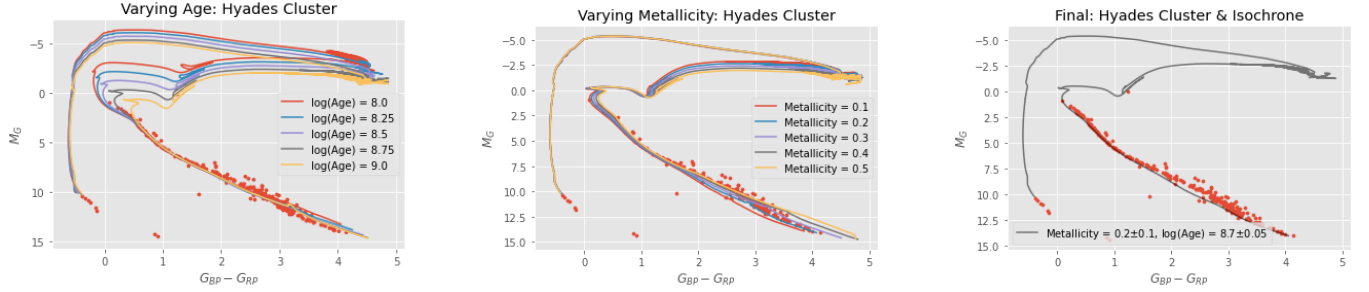


Figure 6: The effect of variation of Age, Metallicity, and corresponding final selection of isochrone corresponding to the Hyades cluster.

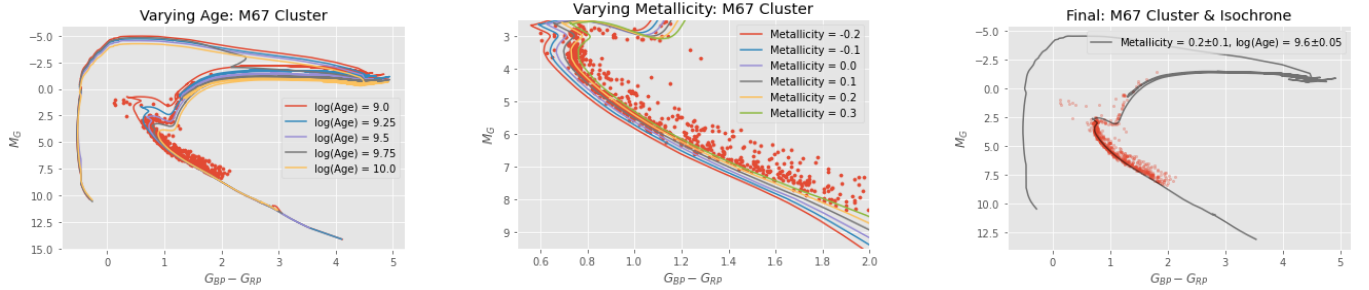


Figure 7: The effect of variation of Age, Metallicity, and corresponding final selection of isochrone corresponding to the M67 cluster.

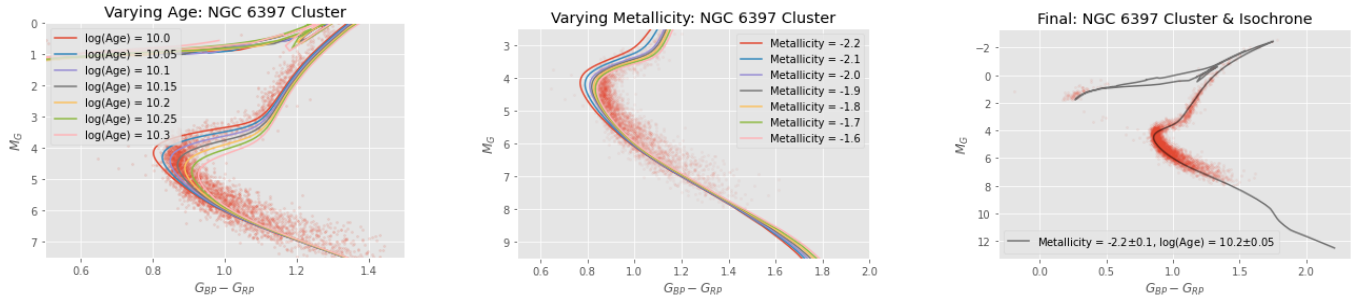


Figure 8: The effect of variation of Age, Metallicity, and corresponding final selection of isochrone corresponding to the NGC 6397 cluster.

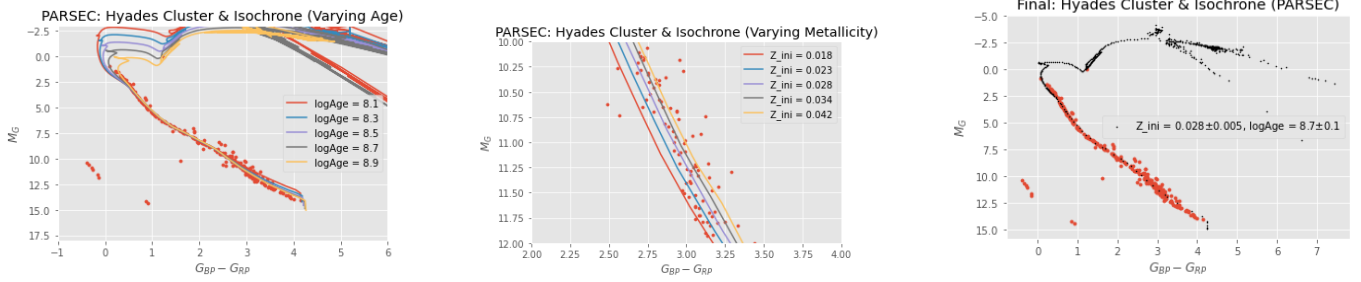


Figure 9: The effect of variation of Age, Metallicity, and corresponding final selection of isochrone corresponding to the Hyades cluster, using PARSEC.

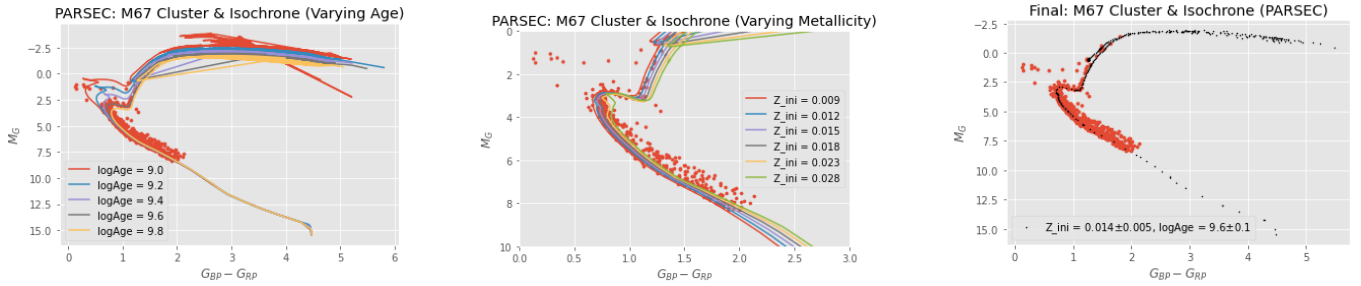


Figure 10: The effect of variation of Age, Metallicity, and corresponding final selection of isochrone corresponding to the M67 cluster, using PARSEC.

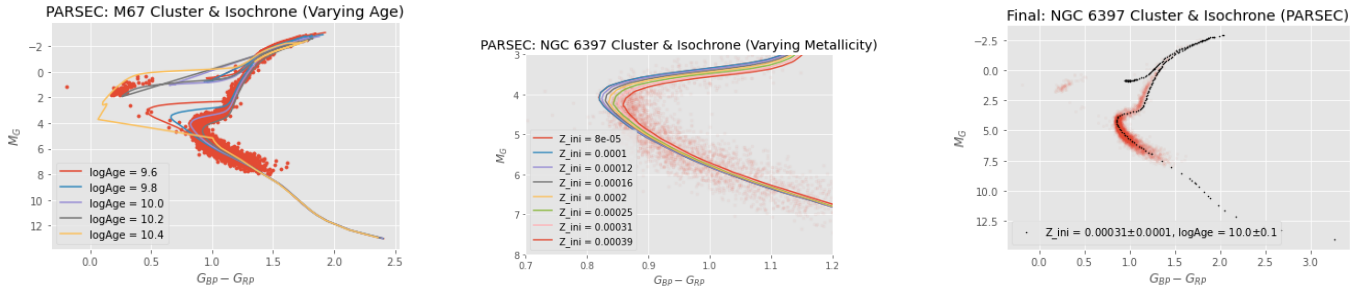


Figure 11: The effect of variation of Age, Metallicity, and corresponding final selection of isochrone corresponding to the NGC 6397 cluster, using PARSEC.

For PARSEC, we chose identical search ranges as compared to MIST, and performed an identical analysis. We chose the best fit metallicities and ages for each case and present a final image of the best fit for each case.

For Hyades, we find a Z_{ini} of 0.028, and a $\log(\text{Age})$ of 8.7 ± 0.1 . For M67, the best fit was a Z_{ini} of 0.014, and a $\log(\text{Age})$ of 9.6 ± 0.1 . For NGC 6397, we found a Z_{ini} of 0.00031, $\log(\text{Age})$ of 10.0 ± 0.1 . The agreement is close, but not always exact. We also find significant differences between the isochrones of MIST and PARSEC in the late-evolutionary stages of the star, with MIST showing a path toward white dwarf creating, while PARSEC drifts to redder colors. Figures for Parsec Isochrones are 9, 10, 11.

REFERENCES

- Gaia Collaboration, Babusiaux, C., van Leeuwen, F., et al. 2018, A&A, 616, A10, doi: [10.1051/0004-6361/201832843](https://doi.org/10.1051/0004-6361/201832843)
- Wenger, M., Ochsenbein, F., Egret, D., et al. 2000, A&AS, 143, 9, doi: [10.1051/aas:2000332](https://doi.org/10.1051/aas:2000332)